

**Datashare 45:**

*Sea level and vertical motion of continents from dynamic earth models since the Late Cretaceous*

**Sonja Spasojevic and Michael Gurnis**

AAPG Bulletin, v. 96, no. 11 (November 2012), pp. 2037–2064

Copyright ©2012. The American Association of Petroleum Geologists. All rights reserved.

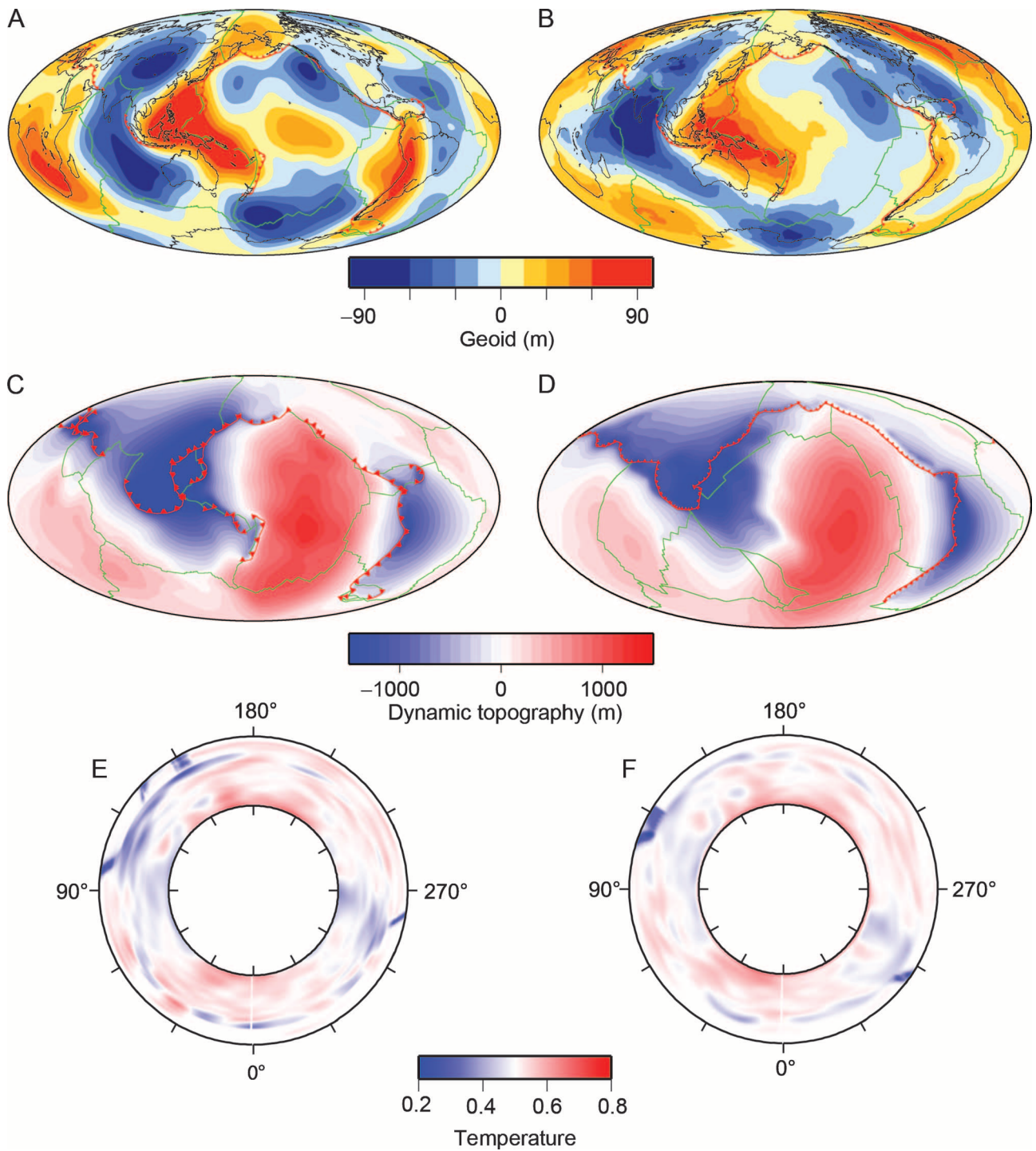


**Figure 2.** Dynamic topography and geoid prediction for model M3. (A) Predicted geoid at 0 Ma. (B) Observed geoid. (C–D) Predicted dynamic topography at 0 Ma (C) and 80 Ma (D). (E–F) Global equatorial spherical cross section through nondimensional temperature field at 0 Ma (E) and 80 Ma (F).

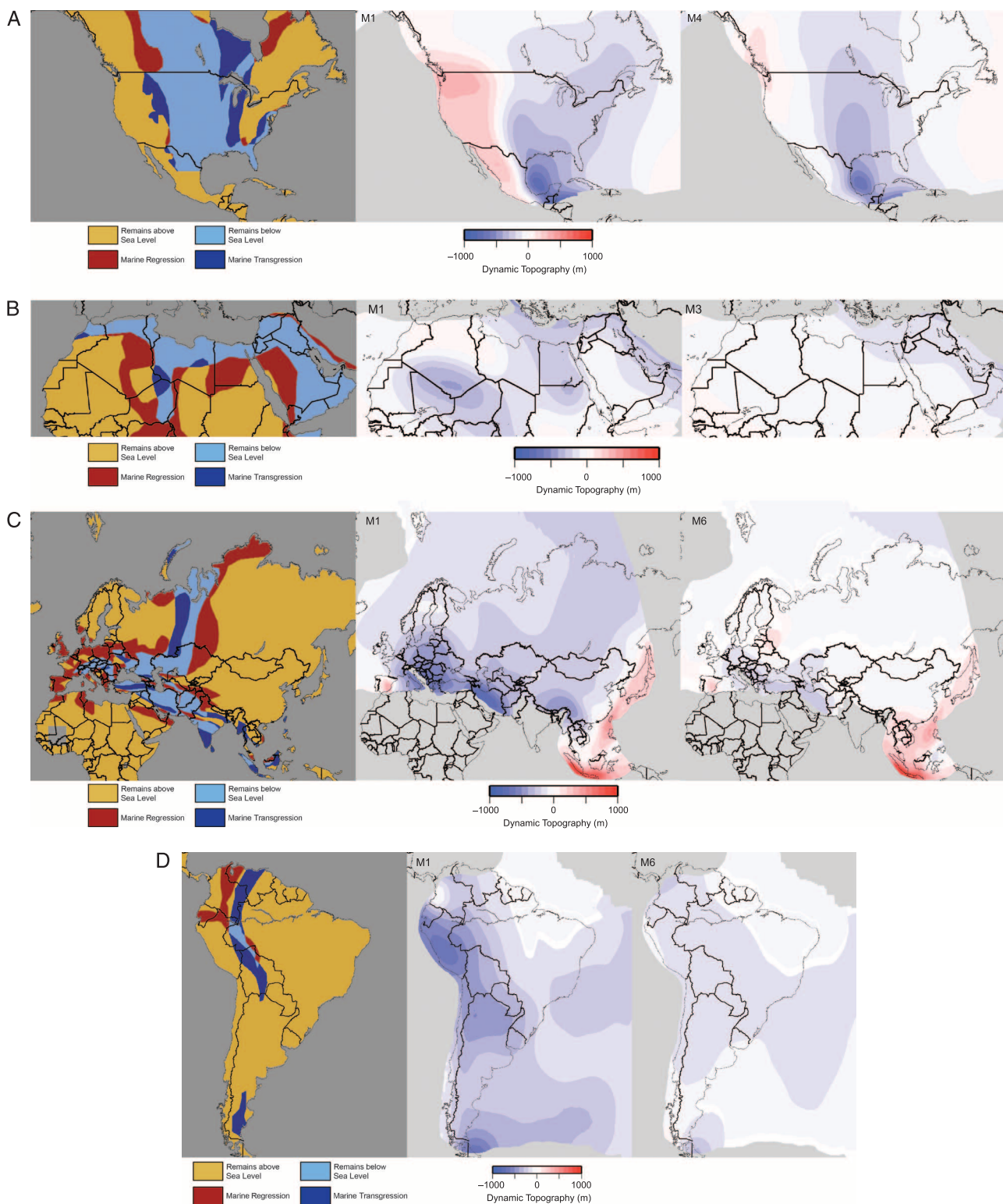
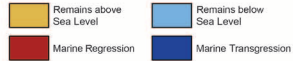
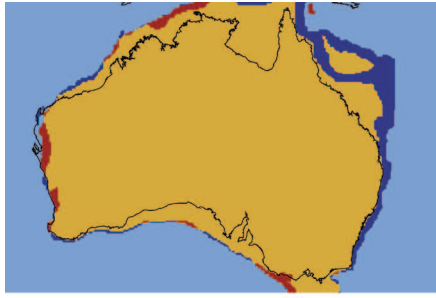


**Figure 4.** Inferred relative sea level change in the Late Cretaceous for North America (A), northern Africa and Arabia (B), Eurasia (C), South America (D), and Australia (E). The first image in panels A to E represents relative sea level inferred from paleogeography using reconstructions at 70 and 90 Ma (Smith et al., 1994) (A); late Santonian–Maastrichtian and latest Albian–early Senonian (Guiraud et al., 2005) (B); 65 and 90 Ma (Blakey, 2010) (C–D); and 60 and 77 Ma (Langford et al., 1995) (E). Relative vertical motions inferred from dynamic models are shown, with “M” corresponding to the specific hybrid model (Table 1).

E



M3

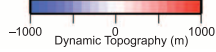
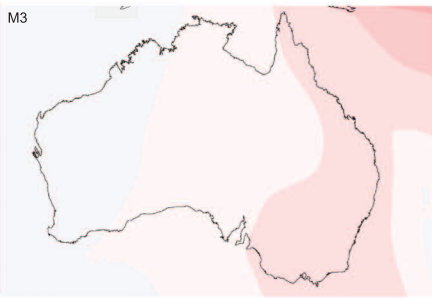


**Figure 4.** Continued.

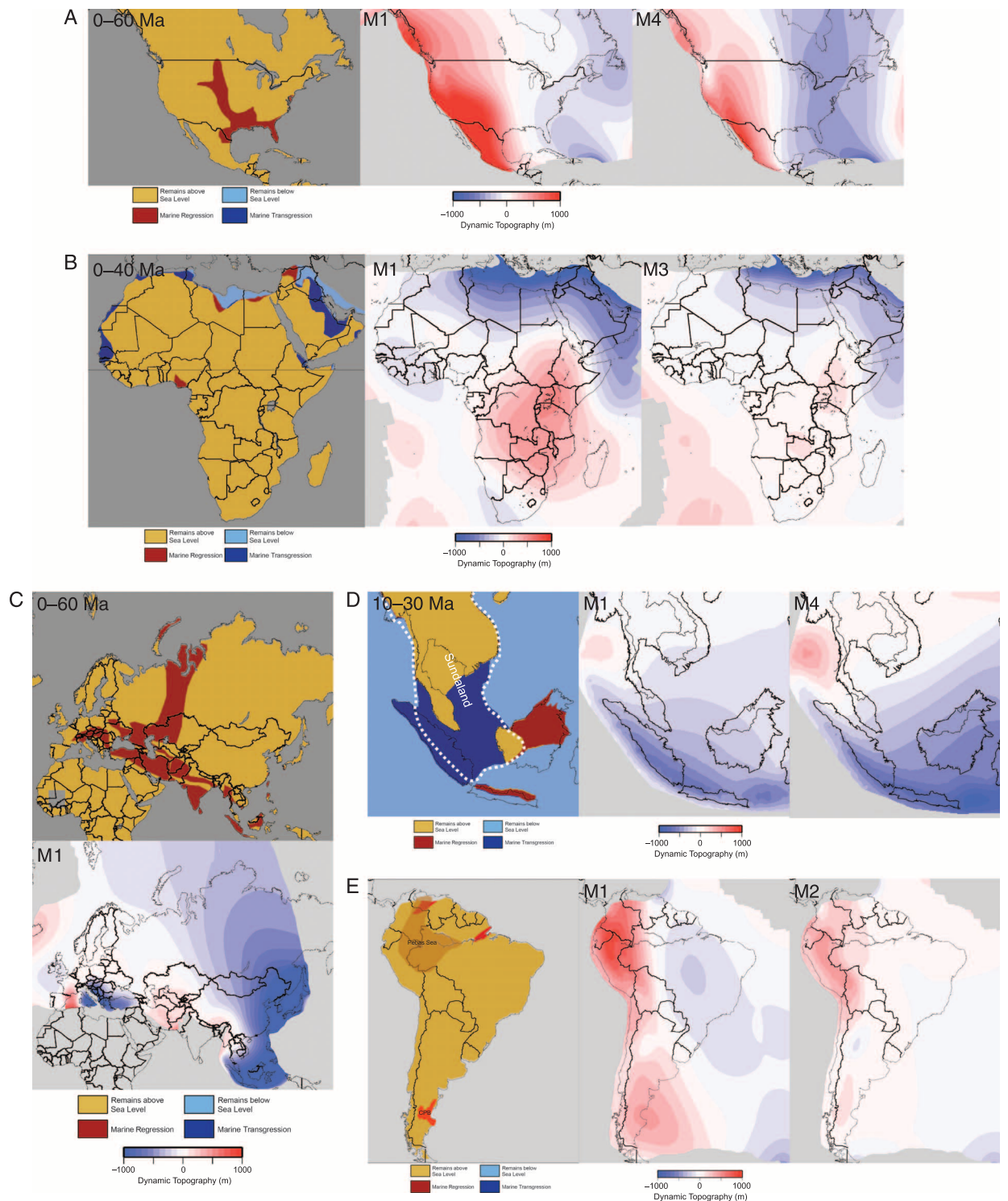


**Figure 5.** Inferred relative sea level change in the Cenozoic: 0 to 60 Ma in North America (A); 0 to 40 Ma in northern Africa and Arabia (B); 0 to 60 Ma in Eurasia (C); 10 to 30 Ma in Southeast Asia (D); 0 to 20 Ma in South America (E); and 0 to 60 Ma in Australia (F). The first image in panels A to E represents relative sea level inferred from paleogeography using reconstructions at 60 Ma (Smith et al., 1994) (A); Miocene and early-middle Oligocene in northern Africa (Guiraud et al., 2005) and 35 Ma in southern and central Africa (Blakey, 2010) (B); 65 Ma (Blakey, 2010) (C); middle Miocene and late Oligocene (Hall and Morley, 2004) (D); 20 Ma (Blakey, 2010) (E), and 60 Ma (Langford et al., 1995) (F). Relative vertical motions inferred from dynamic models are shown, with “M” corresponding to the specific hybrid model (Table 1). CPB = central Patagonian Basin. The legend is the same as for Figure 4.

F

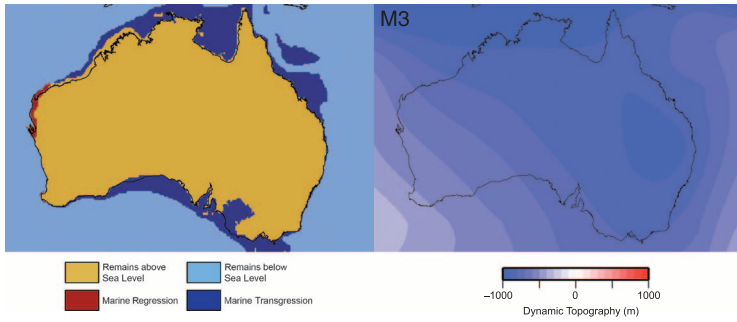
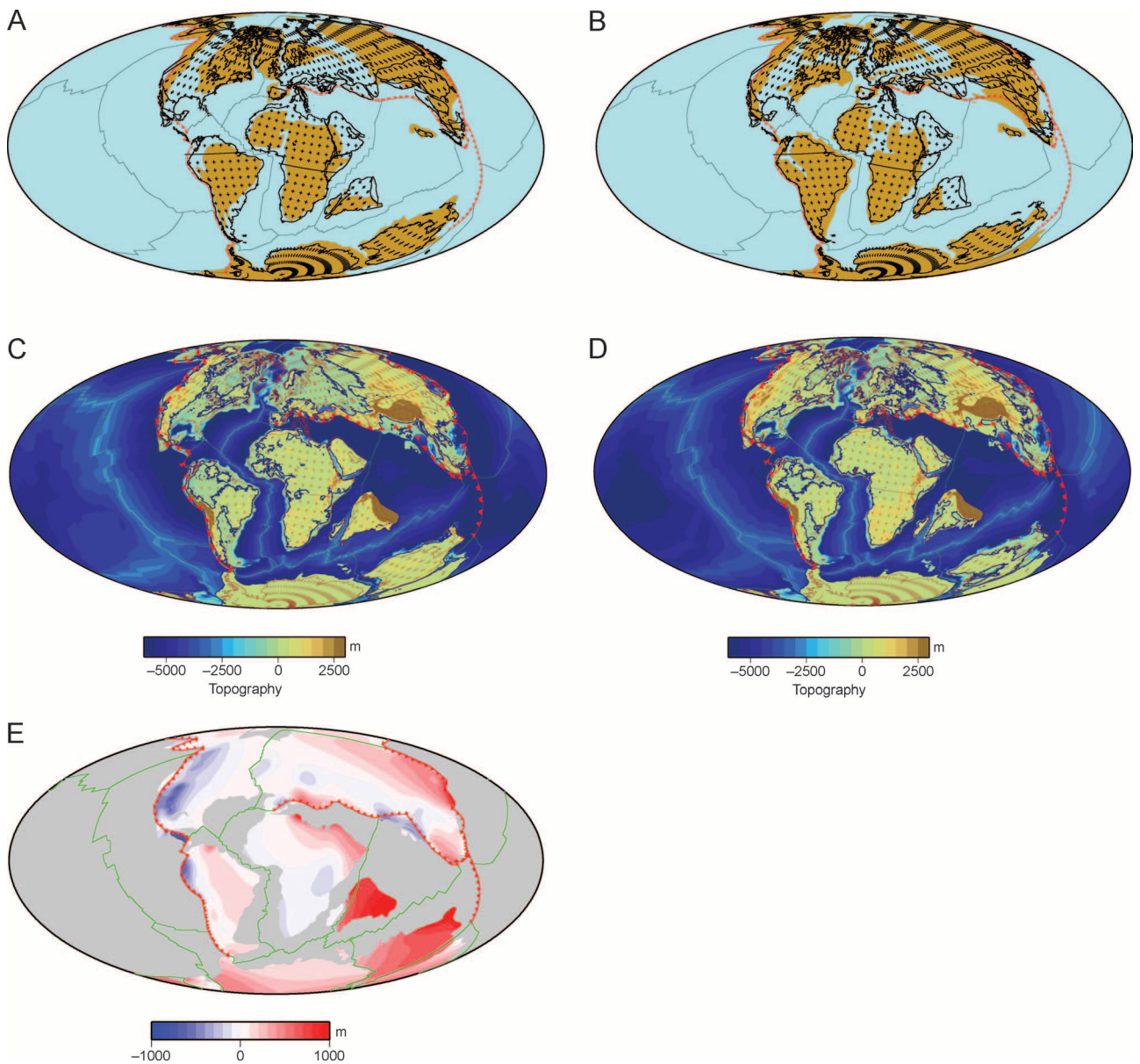
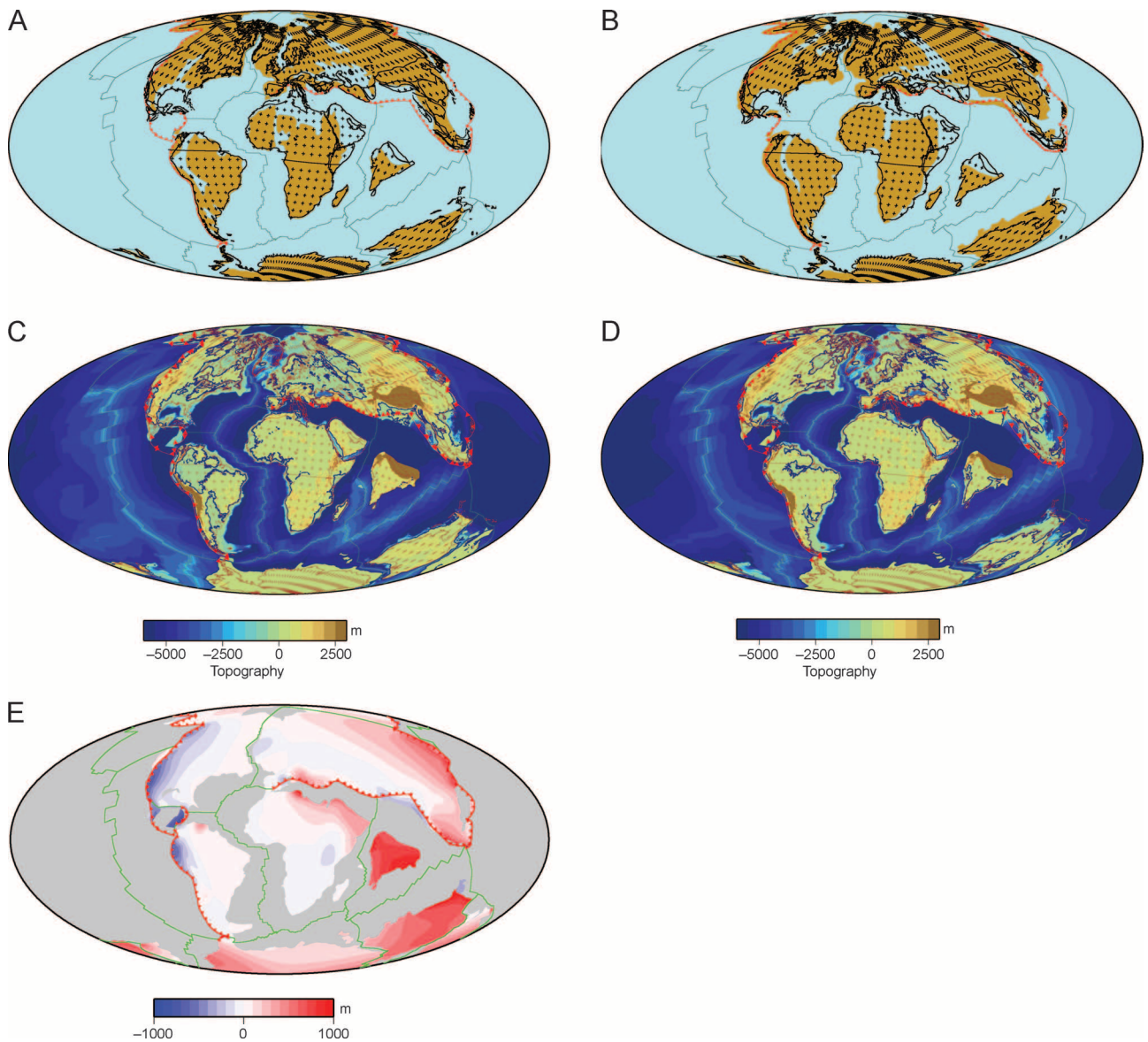


Figure 5. Continued.



**Figure 6.** Late Cretaceous global sea level predictions. Paleogeographic reconstructions at 80 Ma (Smith et al., 1994) (A) and 90 Ma (B) (Blakey, 2010), showing reconstructed marine regions in light blue and land regions in brown. (C) DYN-OFA flooding predictions (80 Ma) accounting for the changing age of the ocean floor, dynamic topography, and geoid, using model M3 (Table 2). (D) OFA flooding predictions (80 Ma) accounting only for the changing age of the ocean floor using the half-space model without flattening (Parsons and Sclater, 1977). (E) Difference between dynamic topography in the past (80 Ma) and present-day predicted dynamic topography for model M3. The dark blue lines on panels C and D show a predicted shoreline.



**Figure 7.** Early Cenozoic global sea level predictions. Paleogeographic reconstructions at 60 Ma (A) (Smith et al., 1994) and 65 Ma (B) (Blakey, 2010), showing reconstructed marine regions in light blue and land regions in brown. (C) DYN-OFA flooding predictions (60 Ma) accounting for the changing age of the ocean floor, dynamic topography, and the geoid and using model M3 (Table 2). (D) OFA flooding predictions (60 Ma) accounting only for the changing age of the ocean floor using the half-space model without flattening (Parsons and Sclater, 1977). (E) Difference between dynamic topography in the past (60 Ma) and present-day predicted dynamic topography for model M3. The dark blue lines on panels C and D show a predicted shoreline.

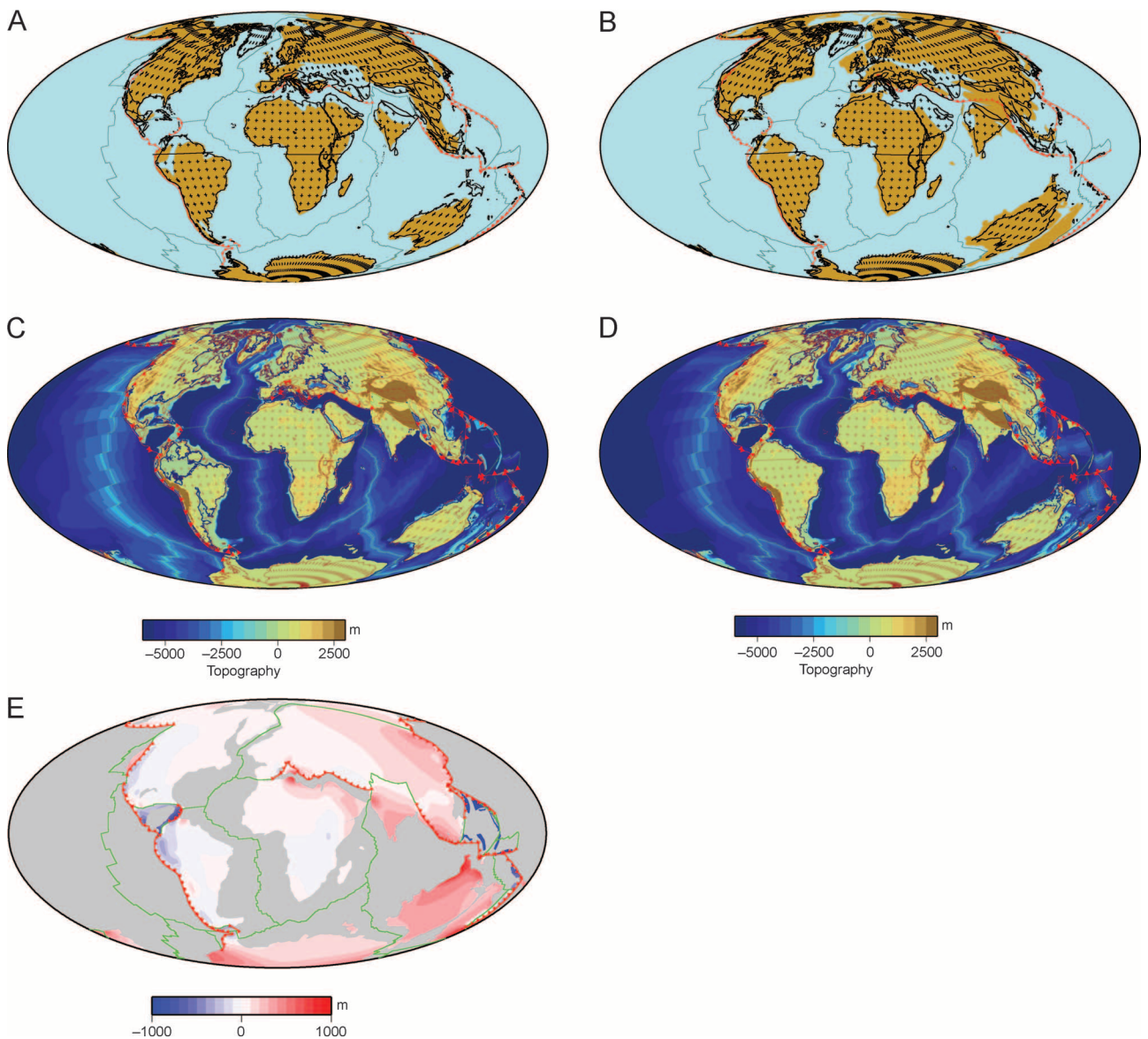


**Figure 8.** Global sea level predictions (30 Ma). Paleogeographic reconstructions at 30 Ma (A) (Smith et al., 1994) and 35 Ma (B) (Blakey, 2010), showing reconstructed marine regions in light blue and land regions in brown. (C) DYN-OFA flooding predictions (30 Ma) accounting for the changing age of the sea floor, dynamic topography, and the geoid and using model M3 (Table 2). (D) OFA flooding predictions (30 Ma) accounting only for the changing age of the sea floor using the half-space model without flattening (Parsons and Sclater, 1977). (E) Difference between dynamic topography in the past (30 Ma) and present-day predicted dynamic topography for model M3. The dark blue lines on panels C and D show a predicted shoreline.

## APPENDIX 1: VISCOSITY, RESOLUTION, AND OTHER MODEL PARAMETERS

The effective viscosity is defined as

$$\eta = \eta_0 \exp\left(\frac{E^*}{T + T_0} - \frac{E^*}{0.5 + T_0}\right) \quad (3)$$

where  $\eta$  is effective viscosity,  $\eta_0$  is reference viscosity (Table 4),  $E^*$  is activation energy divided by the product of the gas constant  $R$  ( $8.314 \text{ JK}^{-1}\text{mol}^{-1}$ ) and temperature scaling  $T_S$  (3000 K),  $T$  is nondimensional temperature, and  $T_0$  is a temperature offset. We use values of  $E^* = 10$  to 30 and  $T_0 = 0.5$  to 1.0 for both upper and lower mantles. Important parameters of hybrid models are given in Table 4.

The resolution is approximately 50 km (31 mi), with the 129 by 129 nodes per CitcomS cap in map view and 65 nodes in the radial direction with refinement in the upper mantle and lithosphere. Resolution testing with several different spatial and radial resolutions showed that this resolution was sufficient (Spasojevic et al., 2010b).

Ocean bathymetry for the half-space model (Parsons and Sclater, 1977) with flattening after 70 Ma is defined as

$$d = 2500 \text{ m} + 350 \text{ m}\sqrt{t} \quad t \leq 70 \text{ Ma} \quad (4)$$

**Table 4.** Parameters of Hybrid Models

Parameter	Symbol	Value
Ambient mantle density	$\rho_m$	3340 kg/m <sup>3</sup>
Water density	$\rho_w$	1000 kg/m <sup>3</sup>
Reference viscosity	$\eta_0$	$1 \times 10^{21}$ Pa s
Thermal diffusivity	$\kappa$	$10^{-6}$ m <sup>2</sup> /s
Coefficient of thermal expansion	$\alpha$	$3 \times 10^{-5}$ 1/K
Gravitational acceleration	$g$	9.81 m/s <sup>2</sup>
Radius of Earth	$R$	6371 km

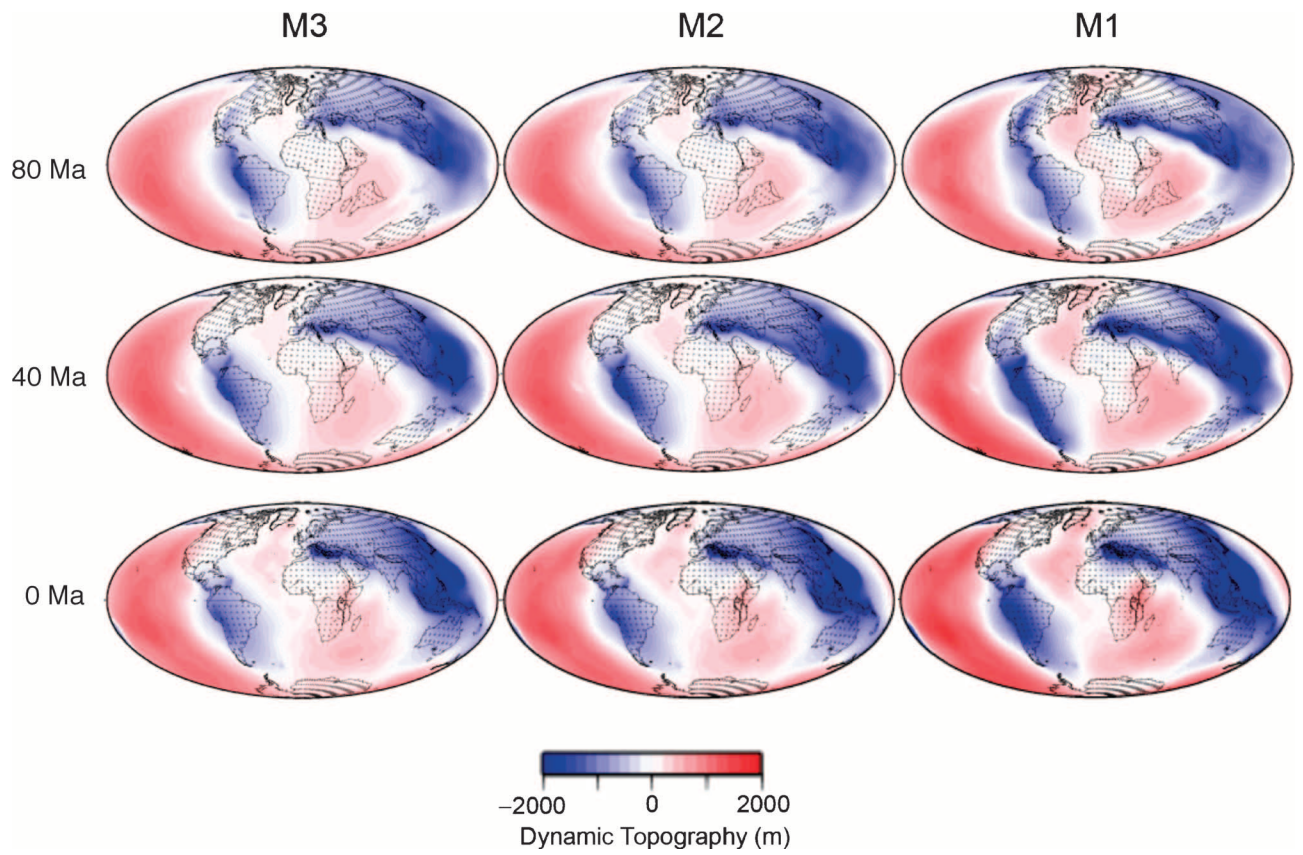
$$d = 6400 \text{ m} + 3200 \text{ m} \exp(-t/62.8) \quad t > 70 \text{ Ma} \quad (5)$$

where  $d$  is the depth of ocean floor in meters,  $t$  is the age of sea floor in million years. For plate model GDH-1 (Stein and Stein, 1992), the ocean bathymetry is defined as

$$d = 2600 \text{ m} + 365 \text{ m}\sqrt{t} \quad t = 0 - 20 \text{ Ma} \quad (6)$$

$$d = 5651 \text{ m} - 2473 \text{ m} \exp(-0.0278t) \quad t > 20 \text{ Ma} \quad (7)$$

## APPENDIX 2: PREDICTED DYNAMIC TOPOGRAPHY



Predicted dynamic topography for 80, 40, and 0 Ma for models M3, M2 and M1.

### APPENDIX 3: DIFFERENTIAL DYNAMIC TOPOGRAPHY

